Absolute, spatially resolved, in situ CO profiles in atmospheric laminar counter-flow diffusion flames using 2.3 μm TDLAS

Steven Wagner · Moritz Klein · Trupti Kathrotia ·
Uwe Riedel · Thilo Kissel · Andreas Dreizler ·
Volker Ebert

Abstract We developed a new, spatially traversing, direct tunable diode laser absorption spectrometer (TDLAS) for quantitative, calibration-free, and spatially resolved in situ measurements of CO profiles in atmospheric, laminar, non-premixed CH_4/air model flames stabilized at a Tsuji counter-flow burner. The spectrometer employed a carefully characterized, room temperature distributed feedback diode laser to detect the R20 line of CO near 2,313 nm ($4,324.4$ cm^{-1}), which allows to minimize spectral CH_4 interference and detect CO even in very fuel-rich zones of the flame. The burner head was traversed through the 0.5 mm diameter laser beam in order to derive spatially resolved CO profiles in the only 60-mm wide CH_4/air flame. Our multiple Voigt line Levenberg–Marquardt fitting algorithm and the use of highly efficient optical disturbance correction algorithms for treating transmission and background emission fluctuations as well as careful fringe interference suppression permitted to achieve a fractional optical resolution of up to 2.4×10^{-4} OD (1σ) in the flame (T up to 1,965 K). Highly accurate, spatially resolved, absolute gas temperature profiles, needed to compute mole fraction and correct for spectroscopic temperature dependencies, were determined with a spatial resolution of 65 μm using ro-vibrational N_2-CARS (Coherent anti-Stokes Raman spectroscopy). With this setup we achieved temperature-dependent CO detection limits at the R20 line of 250–2,000 ppmv at peak CO concentrations of up to 4 vol.%. This permitted local CO detection with signal to noise ratios of more than 77. The CO TDLAS spectrometer was then used to determine absolute, spatially resolved in situ CO concentrations in the Tsuji flame, investigate the strain dependence of the CO Profiles and favorably compare the results to a new flame-chemistry model.

S. Wagner · M. Klein · T. Kissel · A. Dreizler · V. Ebert
Fachgebiet Reaktive Strömungen und Messtechnik,
Center of Smart Interfaces, Technische Universität Darmstadt,
Petersenstr. 32, 64287 Darmstadt, Germany

S. Wagner · V. Ebert (✉)
Physikalisch-Technische Bundesanstalt,
Bundesallee 100, 38116 Braunschweig, Germany
e-mail: volker.ebert@ptb.de

T. Kathrotia · U. Riedel
Universität Stuttgart and Institute of Combustion Technology,
German Aerospace Center, Pfaffenwaldring 38-40,
70569 Stuttgart, Germany

1 Introduction

Light emitted by flames via chemiluminescence (CL) offers a completely passive possibility to realize a low-cost active control and optimization of technical combustion processes. One of the molecular species responsible for CL emission is exited CO_2^* whose absolute concentrations are very difficult to quantify. In combustion processes one of the main precursors for the excited CO_2^* is carbon monoxide (CO). Following Najm et al. [1] excited CO_2^* is only created by a minor oxidation step ($CO + O^3P + M \rightarrow CO_2{}^3B_2 + M$). This reaction path does not contribute significantly to the conversion of the fuel to CO_2. But CO_2^* formation from CO is a very important reaction for the validation of enhanced CL models, which makes the CO distribution in the flame front a very important information to validate improved CL reaction mechanisms.

Of course CO also plays an important role as a marker for the kinetic progress in the flame and as an indicator for the efficiency of the combustion. CO is solely oxidized by the hydroxyl radical (OH) $CO + OH \rightarrow CO_2 + H$ and

significantly involved in the heat release of the flame by the oxidation reaction [2, 3]. According to that the product of the CO and OH concentrations may also be used to reveal the location of maximum heat release.

The importance of CO as an indicator for the reaction zone, the reaction progress, fuel consumption, and the reaction kinetics makes this molecule an ideal measurement parameter for the validation of combustion models. Beside this high relevance concerning the simulation of chemical processes in the combustion environment, CO has also a direct influence on the measurement techniques, like laser-induced fluorescence (LIF), which is also a prominent optical diagnostic method for absolute concentration measurements. It can appear either as a measurement parameter [4, 5] or as a collision partner [6], which reduces the population number density of the target species due to inelastic collisions of the molecules termed quenching [7]. The quenching of the measurement signal has to be accounted for by an extensive calibration or by complex correction algorithms. For this purpose the knowledge of the absolute CO mole fraction in heated gas flows or laminar standard flames is necessary. Hence there is a high demand for absolute and calibration-free CO measurements.

The detection of CO mole fractions was frequently demonstrated in various combustion systems from power plants [8, 9] to lab flames [4, 10–17]. Numerous measurement techniques like LIF [4, 14], Raman spectroscopy [17, 18], gas chromatography [19, 20], mass spectrometry [16, 17], extractive TDLAS [11], TDLAS [8, 9, 13, 21] and diode laser wavelength modulation spectroscopy [12] have been applied. Wang et al. [12] detected CO in a premixed, McKenna type, atmospheric flame, but needed a calibration process to get absolute values. Webber et al. (TDLAS [13]) probed (A) the cold exhaust gases where no CH_4 interference has to be taken care of and (B) the combustion region, however, without spatial resolution and without detailed discussion of the signal uncertainties. Further, the setup was not designed to provide any spatial resolved CO profile but only a spatially integrated value. The results were not compared with detailed chemical reaction models.

In this publication the first absolute, calibration free and spatially resolved in situ carbon monoxide mole fraction measurements in an atmospheric, Tsuji-type, diffusion flame are shown. The experimental CO spatial profiles are compared with simulated CO profiles based on new and improved flame-chemistry model [2].

2 Burner setup and flame structure

The measurement of the CO mole fraction was realized in a modified CH_4/air Tsuji burner (Type IV) [20, 22, 23] with a stabilized counter-flow diffusion flame. A U-shaped flame is formed by radial ejecting of methane trough a downwards oriented cylindrical, sintered brass matrix with a radius, $r_{burner} = 20$ mm, into an upward directed, laminar air-stream. In this counter-flow configuration a flow stagnation point is formed in which the downward velocity vector of the fuel flow and the upward velocity vector of the air flow compensate to zero (Fig. 1). The importance of this burner comes from: (A) that the flame and burner can be treated as a completely one-dimensional problem along the vertical line from the lowest point of the burner surface through the flow stagnation point. This drastically simplifies the simulation of the flow distribution and the flame-chemistry interaction, and explains the importance of this burner configuration for the validation of flame-chemistry models. (B) Simultaneously the flame is very homogeneous in temperature and chemistry along lines that are parallel to the cylinder axis and that intersect with the vertical line through the stagnation point. This on the other hand makes this burner type nearly ideal for laser based absorption techniques. (C) The Tsuji burner allows varying in a very controlled fashion an important parameter for turbulent flame description, the stagnation velocity gradient (strain rate) of the flame. *The strain rate (a), which is a key parameter for turbulent flame models, is defined as*

Fig. 1 Schematic of a Tsuji-type burner head. The fuel is ejected through the sintered brass material and forms in the counter propagating air flow a cylindrical flame front coaxially located around the brass cylinder
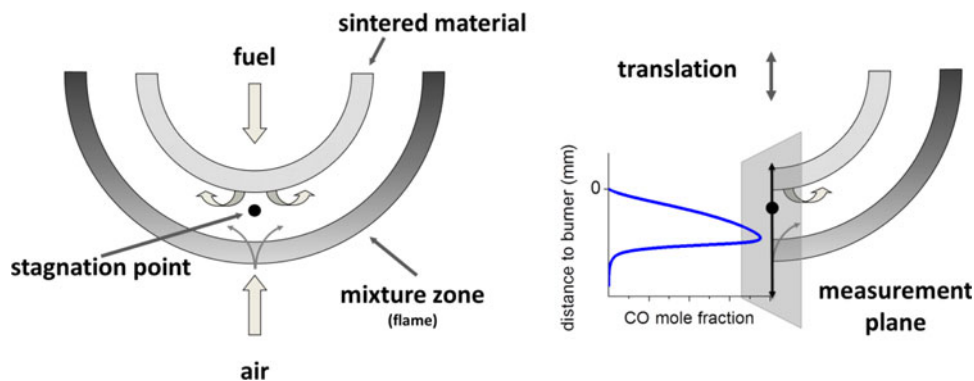
$$a = 2 \cdot v_{air}/r_{burner} \tag{1}$$

The strain is varied by changing the fuel ejection velocity (in this paper between 0.18 and 0.25 m/s) and the air velocity. As an unavoidable consequence this also changes the distance between the main reaction zone and the burner surface (defined by the lower surface of the brass matrix).

Validation of flame-chemistry models in a Tsuji burner is therefore realized by experimentally analyzing in comparison to the model results of the flame thermo-chemistry (i.e., temperature and species concentration) along the vertical line through the stagnation point. Species profiles can then be measured by spatially scanning laser absorption spectroscopy and has been realized previously, e.g., for OH using UV lasers [24].

A common problem of the Tsuji configuration which limits the flame flatness and thus the assumption of homogeneous thermo-chemical conditions along the absorption path, is the buoyancy driven upward curvature of the flame front at the both ends of the fuel cylinder and the insufficiently defined flame "ends", by the so-called end-flames [25], which also cause beam steering. To further reduce these problems and ensure a uniform, flat flame without curved end-flames, we modified the classical Tsuji burner design by adding N_2-co-flow nozzles on both ends of the flame for better balance the flow fields at the cylinder ends and to pinch-off the end-flames. In contrast to the standard Tsuji configuration our improved design generates much flatter flames that are much better suited for absorption measurements [25]. The absorption path length was derived by scanning along the cylinder and measuring the CH_4 absorption signal [26] perpendicular to it. The relative strong decrease of the CH_4 absorption at the flanks defines the very homogeneous 60 mm long absorptions path with an uncertainty of 1 %.

3 Direct absorption spectroscopy

For the calibration-free and absolute measurement of CO mole fractions we employed our direct tunable diode laser absorption spectroscopy (dTDLAS) [9, 27, 28] variant, which permits in situ detection of species concentrations, gas temperatures, or gas residence time distributions [8, 9, 27–30]. This is a beneficial approach especially in harsh environments where calibration is problematic. In dTD-LAS the dc-coupled detector signal in contrast to Wavelength Modulation Spectroscopy (WMS), Frequency Modulation Spectroscopy (FMS) or dual beam techniques is directly digitized and used for the subsequent data evaluation thereby including all offsets and disturbances. For the recovery of the absorption line shape wavelength

scanning via a linear ramp-like laser current modulation is used.

To determine spatially resolved species profiles we vertically translate the burner within the air duct and through the spatially fixed laser beam. This is done in 100 μm steps via a software controlled DC motor connected to a high-resolution translation stage. The smallest step size of the motor corresponds to 0.5 μm.

In dTDLAS the diode laser beam is directed through the detection volume and the resulting light loss is detected by a photo diode. Assuming a thermo-chemically homogeneous absorbing medium provided by the flat flame we use the extended Lambert–Beer law [31] to describe and analyze the absorption process:

$$I(\lambda) = E(t) + I_0(\lambda) \cdot \mathrm{Tr}(t) \cdot \exp[-S(T) \cdot g(\lambda - \lambda_0) \cdot N \cdot L] \tag{2}$$

Therein $I_0(\lambda)$ denotes the initial and $I(\lambda)$ the transmitted laser intensity. The molecular absorption signal is described by the temperature-dependent line strength $S(T)$, the absorber number density N, the absorption path length L, and the normalized line shape function $g(\lambda - \lambda_0)$, which is centered at wavelength λ_0. $\mathrm{Tr}(t)$ terms temporal fluctuations of the broadband overall transmission that may be present. These fluctuations in general can be caused by broadband absorption, light scattering by particles or beam steering. $E(t)$ accounts for background radiation, which would increase the detected signal and thus must be subtracted from the photo detector signal in order to correctly determine the transmitted laser light.

4 In-flame TDLAS spectrometer setup

Due to the high amount of fuel (CH_4) and water (H_2O) present in certain sections of the flame many CO lines suffer severe interference by the dense CH_4 combination band at 2.3 μm. Thus, it is necessary to select an optimal, i.e., spectrally unobscured CO transition with sufficient line strength: particularly interesting is the spectral region between 4,320 and 4,325 cm^{-1} (Fig. 2).

Our proprietary line selection procedure shows under combustion conditions two CO lines with little CH_4 background as well as only weak interfering H_2O transitions. Here, CO-R19 seems to be the better choice due to the smallest CH_4-background. Nevertheless, we chose the CO-R20 line due to the slightly stronger CH_4 structure nearby which can be used for subtracting the methane background via a multiline spectrum fit. To do this, the CH_4 spectrum was calculated for the full modulation range and fitted to the measured data nearby the CO-R20 line. This background reduction method proved to be quite
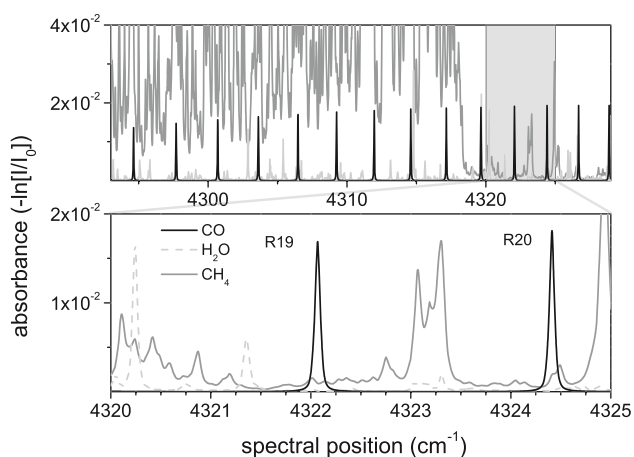
Fig. 2 HITRAN08/HITEMP10 based spectral simulation [32, 33] for the range of the first CO overtone band at 2,320 nm. In the gap between 4,320 and 4,350 cm^{-1} one can find CO lines with less crosstalk from CH_4 and H_2O transitions. The CO-R20 can therefore be used in flame regions even with rather high CH_4 or H_2O mole fractions. The spectra are simulated for typical flame conditions (1,950 K, 1 atm, 0.06 m, c[CO] 5 vol.%, c[H_2O] 18 vol.% as well as 900 K, 1 atm, 0.06 m, c[CH_4] 50 vol.%)

efficient and thus lead significantly higher signal-to-noise ratios (up to three times) and a better accuracy and precision for the line area extraction.

To estimate the relative influence of temperature errors we analyze the density-normalized temperature dependence ($S(T)/T$) of the CO-R20 line strength (Fig. 3) which shows over the full temperature range in the flame (500 K < T_{CO} < 2,000 K) temperature coefficients from 0.3 to 0.05 %/K. Around the $S(T)/T$ maximum near 600 K the temperature dependence is negligible, whereas for the further distant temperatures the influence of the measurement uncertainty of the temperature is still small. This is beneficial for flame conditions with large temperature gradients or for the case of enhanced uncertainties in temperature determination.

Nevertheless, it is important to ensure high accuracy and precision of the temperature measurement to minimize the CO concentration uncertainty. Therefore, we used CARS (N_2 ro-vibrational coherent anti-Stokes Raman spectroscopy) in the planar BOXCARS configuration, which

requires that the laser beam of a frequency doubled Nd:YAG laser (532 nm) and a modeless broadband dye laser (607 nm) are phase-matched within the surface [34]. With that technique we determined absolute, spatially resolved ($\Delta x = 65 \mu m$) temperature profiles perpendicular to the burner surface along the vertical line through the stagnation point with relative temperature uncertainties of only 1.6–2 %.

After the line selection procedure we selected as light source for the absorption spectrometer a single mode, continuously tunable, near infrared distributed feedback (DFB) diode laser (Nanoplus) with an emission wavelength near 2.313 μm. This DFB diode lasers show a typical emission line width in the low MHz to high kHz showing high spectral stability and a well-defined, Gaussian beam shape. The lasers' spectral purity was specified by manufacture to be better than 30 dB. The stability and static as well as dynamic wavelength tuning characteristics were measured in our group [9] (Fig. 4).

For the flame profile measurement the laser wavelength was scanned over a 1.77 cm^{-1} spectral interval with a repetition rate of 140 Hz, using a triangular laser current modulation. The laser light was collimated by an aspheric lens (beam diameter = 1 mm). Gold-coated planar bending mirrors directed the collimated beam through two 0.5-mm pin holes placed on both sides of the flame (separated by 100 mm) for beam shaping and suppression of the flame radiation. Without using any deconvolution techniques these pin holes define our spatial resolution to about 0.5 mm. A 1″, 90° off-axis parabolic mirror collected the laser light and focused it onto a double-extended, room-temperature InGaAs detector with 1 mm^2 area. A low-noise transimpedance amplifier (500 kHz bandwidth) converted the resulting photo current in a voltage signal
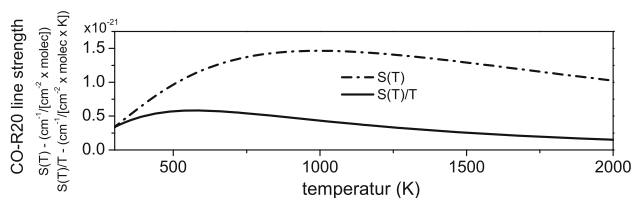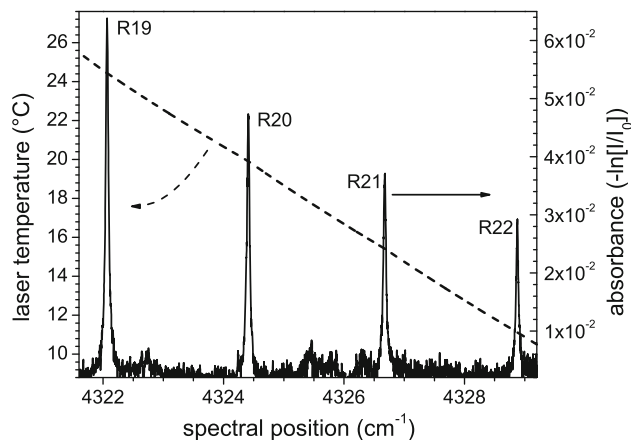

Fig. 3 Temperature dependence of the CO-R20 line strength and the normalized line strength $S(T)/T$ based on HITRAN08 data [32]. Due to weak gradients of $S(T)/T$, the influence of the temperature uncertainty is small along the entire temperature range

Fig. 4 Static wavelength tuning characteristics of the 2.313 μm DFB diode laser. The measured temperature tuning range of 7 cm^{-1} is shown in comparison with a measured CO reference cell spectrum ($L = 10$ cm, $p = 60$ mbar, c[CO] = 100 vol.%, T = 296 K)

which was then digitized with an 18-bit ADC at 140 kSamples/s.

The absorption line profile measured in time space is converted onto a wavenumber axis using the measured dynamic tuning coefficient of the laser. After this a background polynomial of up to 3rd order is used to correct for transmission and emission contributions and the absorption line area of the target line is determined using an in-house, Labview-based, recursive Levenberg–Marquardt algorithm, which uses as a fitting model an array of multiple Voigt line shapes and spectral data from HITRAN2008/HITEMP10 [32, 33]. In addition the fitting process was stabilized by calculating preset values for Doppler as well as for collisional broadening, using measured values of the total pressure, the gas temperature and the measured pressure broadening coefficients of the major local molecular perturbers in the flame. The determined line areas were converted into volume mixing ratios using the ideal gas law and the measured total pressure and CARS temperature.

The measured spatial CO profiles were compared with flame simulation results. The simulations of the non-premixed diffusion flame in one-dimensional Tsuji counter-flow geometry were performed with the flame code INSFLA [35, 36]. The reaction kinetics mechanism used for the simulations in the present work is recently documented in [2]. It has been developed to model basic C_1 to C_4 hydrocarbon fuels under non-sooting condition with added chemiluminating chemistry. The mechanism is validated for global flame parameters such as flame velocities and ignition delay times over wide range of temperatures ($T = 900–2,500$ K), pressures ($p = 0.3–9$ bars), and equivalence ratios ($\varphi = 0.5–3.6$). In addition a more strict validation is obtained by comparison of species profiles

such C_2H_2 [37], CH, C_2, and $^1CH_2$ measured at laminar flame conditions. In the diffusion flames, the mixture composition varies from fuel lean to fuel-rich condition. In methane flames the fuel CH_4 decomposes in a main channel to methyl (CH_3), further to CH_2O, CHO and subsequently CO is formed. At richer conditions there is a competing recombination channel where the CH_3 formed are recombined to ethane and are then oxidized finally forming CO.

5 Results and discussion

Typical examples of transmission-corrected in situ absorption signals for the CO-R20 line are shown in Fig. 5. The spectral background is affected by the CH_4 spectrum particularly in the fuel rich pre-combustion zone. Increasing disturbances from the strong surrounding CH_4 background can be observed at lower temperatures and higher fuel concentrations.

The combination of a Voigt multiline fitting, CH_4 background suppression, optical disturbance correction algorithm and scan averaging for 500 absorption profiles (equivalent to 3.6 s temporal resolution) allowed us to derive highly resolved absorption line profiles in the flame of the Tsuji burner. With CO peak absorbances of 1.85×10^{-2} we achieved a fractional resolution of 2.4×10^{-4} corresponding to a 1σ signal to noise ratio of 77. The fractional resolution was derived from the 1σ average of the total residual as shown in Fig. 5. At a distance of 2.9 mm to the burner surface ($T = 1,880$ K) we determined a CO mixing ratio of 3.7 vol.%, so that the SNR of 77 corresponds to a 1σ detection limit of 480 ppmv equivalent to (54.6 ppmv m $Hz^{-0.5}$).
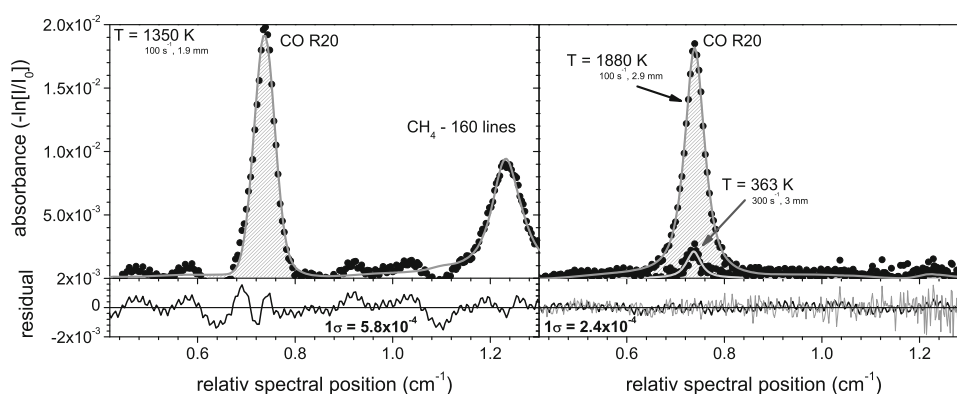

Fig. 5 Measured transmission and emission corrected TDLAS line profile and model fit data of the CO-R20 absorption line (pattern) as well as surrounding CH_4 background, combining 160 CH_4 lines. *Left* Spectrum 1.9 mm distance of the burner surface (at 100 s^{-1}, 1,350 K, c[CO] = 3.3 vol.%, c[CH_4] = 15.7 vol.%), with a fractional absorption of 5.8×10^{-4} (1σ) at 1.98×10^{-2} peak absorbance and a resulting SNR of 34. *Right* 2.9 mm distance of the burner surface (at

100 s^{-1}, 1,880 K, c[CO] = 3.7 vol.%, c[CH_4] = 3.4 vol.%), with a fractional absorption of 2.4×10^{-4} (1σ) at 1.85×10^{-2} peak absorbance and a resulting SNR of 77. Additionally a line profile is shown for low mole fractions, low temperatures and high strains (at 300 s^{-1}, 363 K, 3 mm, c[CO] = 0.29 vol.%, c[CH_4] = 0 vol.%). Small fringes are caused from interference between laser collimator and pin-hole plate at the burner chamber

By vertical translation of the burner head in steps of 0.1 mm, we measured for the first time absolute CO concentration profiles in a Tsuji burner (Fig. 6). This profile agrees well in the range between 1 and 3.2 mm, but differs in the absolute values (<54 %) due to the high concentration gradient of the profile in the up to 4.2 mm. The agreement in shape and position of the experimental profile with the simulations validates the combustion model. Due to the strong Methane background near the burner surface the uncertainty increases but the absolute deviation to the model remains almost constant over a dynamic range of more than two orders of mole fraction (bottom). Only in the range with the highest CO concentration gradient (3–4 mm) the difference between experimental data and simulation is larger. This can be explained by temperature uncertainties, convolution effects due to the spatial resolution of only 0.5 mm (pin-hole diameter) as well as position offsets regarding experimental flow uncertainties. For more detailed discussion of this and further uncertainties regarding the measurement technique we refer the reader to specialized metrological publications [38]. The total CO uncertainties in Fig. 6 are derived from the uncertainties in the absorption path length (± 1 %), the line strength at 296 K (± 2 to ± 5 % HITRAN08 [32]), the temperature measurement (up to ± 2.5 %) and the optical resolution (up to ± 1.5 %). Below 1 mm distance to the burner head the CH_4 background was too strong and due to the temperature-dependent CO line strength as well as low CO concentration level the CO absorption signal was to weak, to get sufficient SNR for a reliable mole fraction determination.
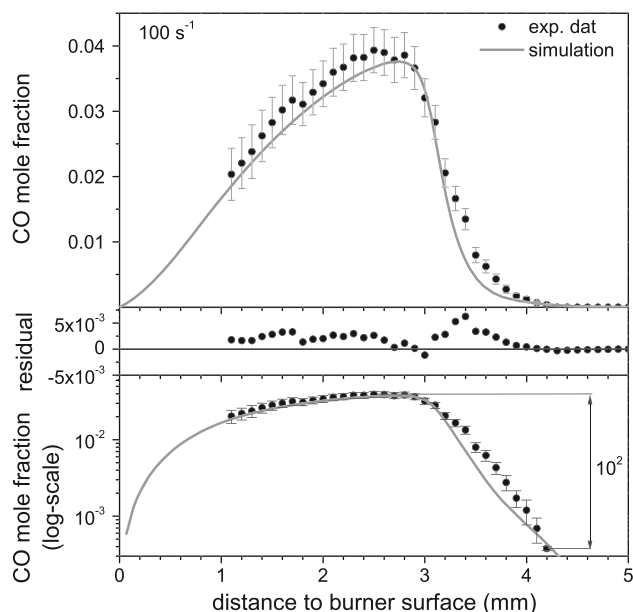
In addition to Fig. 6 we expanded the study and also measured for the first time the strain dependence of the spatial CO distribution in the Tsuji flame. Figure 7 depicts the strain dependence absolute CO concentration profile for four strain rates ranging from 100 to 300 s^{-1} of the Tsuji burner. Over a mole fraction range of two orders only minor differences, due to measurement errors of the fuel ejection rate and the air velocity, can be observed between model and experiment.

With increasing strain rate the CO peak concentration remained constant while the position of the profiles shifted closer to the burner surface. For the highest strain rate ($a = 300 \ s^{-1}$) the fuel ejecting rate had to be increased (from 3 to 5 slpm) to prevent flame extinction as the flame got to close to the burner head. As expected this caused a shift of CO profile position, but also shows higher positions offsets between experiment and simulation. This can be attributed to uncertainties of the CH_4 mass flow controller as well as the heat wire anemometer for the air velocity measurement. Incorrect prediction of the model was tested by variation of the input parameter, but cannot explain the amount or direction of the shift. The CO concentration for the 300 s^{-1} profile seemed not go to zero at the air side, which may be caused by higher noise and quite small peak absorptions in this region. The last trustworthy fit could be made at a distance of 3 mm to the burner surface (Fig. 5 right). The comparison of the profile widths showed only in the high gradient range of the CO concentrations substantial differences due to measurement uncertainties (explained above).

The profiles and the overall trends of peak height, peak position, and slope shape in the experimental CO profiles reproduced the model and its simulation results quite nicely and better than in previous publications [17]. In many locations we agreed very well (i.e., within our uncertainty figures indicated by error bars in the figures) with the model. Biggest deviations happen at the steepest CO slopes where the experimental results may be influenced by spatial offsets and spatial resolution problems. But, model errors are also likely to appear in such critical locations. Therefore, these "locations" generate the highest "optimizing pressure" for the experiment and the model. In order to evaluate the degree of agreement it also has to be taken into account that the TDLAS technique, due to its "absolute" nature, did not have any remaining degrees of freedom to scale our experimental signals to the simulation results, which makes the agreement even more noteworthy. Competing measurement techniques like LIF usually need difficult calibrations or scaling to get absolute mole fraction values [14, 39–41] leading to higher uncertainties and less stringency of the comparison and the value of the comparison to the modelers. Given these boundary conditions our match between simulation and experiment is not

Fig. 6 Spatially resolved CO concentration profiles in the Tsuji counter-flow flame for a strain rate of 100 s^{-1} (*top*)

Fig. 7 Comparison of the measured and simulated CO concentrations profiles for flames with strain rates between 100 and 300 s^{-1}. The experimental data (*dots*) are reproduced very well from the model-based simulation (*line*). The shape, position, and absolute values of the measured profiles agree excellent over a broad range with the simulated data
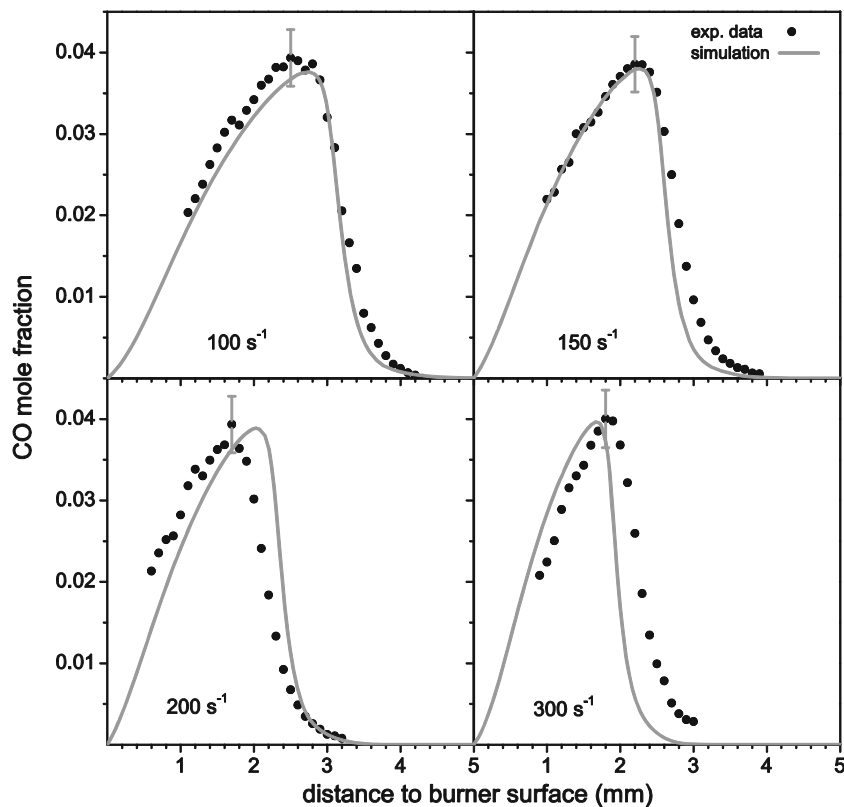
perfect but certainly impressive and of a new quality. The further development of the combustion model will show if the remaining discrepancies can be removed by the model or has to be attributed to the uncertainties or systematic errors of our measurements.

6 Conclusion

We presented the first, absolute in situ TDLAS measurements of CO in the laminar, non-premixed diffusion flame of a Tsuji-type burner. We employed room temperature diode lasers and detectors to detect the R20 CO transition (4,324.4 cm^{-1}) in the 2.3 µm band, which was specially selected to minimize CH_4 interference. Despite the strong temperature and density gradients in the 60-mm wide flame we achieved with direct TDLAS at a temporal resolution of 3.2 s, an optical resolution of up to 2.4×10^{-4} OD (1σ) and a carbon monoxide detection limit of up to 480 ppm (28.8 ppmv m, 54.6 ppmv m Hz$^{-0.5}$). By spatially traversing the burner through the laser beam (step size 100 µm, beam size 500 µm) we measured spatially resolved CO profiles. The strain dependence of the CO concentration profiles was also measured for the first time for two fuel ejection rates and four strain rates. The first comparison of the derived in situ CO data with improved detailed flame simulations showed within our uncertainties

over a CO mole fraction dynamic range of more than two orders of magnitude an excellent agreement between the measured CO TDLAS concentration profiles and the model data. Particularly the determination of absolute mole fraction without any spectrometer calibration step, gas extraction or sample modification is remarkable and provides important data for highly stringent tests and validations of current and future flame models.

7 Outlook

An improvement of the Tsuji flame data will be made by investigating the dependence of the CO profile on fuel composition, on strain rate, and on flame type (partially premixed and premixed flames) as well as via measurement of other species like CH_4, H_2O, or OH also by using our direct TDLAS method.

References

1. H.N. Najm, P.H. Paul, C.J. Mueller, P.S. Wyckoff, Combust. Flame **113**, 312–332 (1998)

2. T. Kathrotia, Reaction kinetics modeling of OH*, CH*, and C2* chemiluminescence. Inaugural-Dissertation, Ruprecht-Karls-Universität Heidelberg, 2011

3. C.I. Heghes, C_1–C_4 hydrocarbon oxidation mechanism. Inaugural-Dissertation, Ruprecht-Karls-Universität Heidelberg, 2006

4. M. Mosburger, V. Sick, Appl. Phys. B **99**, 1–6 (2010)

5. S. Linow, A. Dreizler, J. Janicka, E.P. Hassel, Appl. Phys. B **71**, 689–696 (2000)

6. C.M. Drake, J.W. Ratcliffe, J. Chem. Phys. **98**, 3850–3865 (1993)

7. W. Demtröder, *Laserspektroskopie - Grundlagen Und Techniken, 5. Auflage* (Springer, Berlin, 2007)

8. V. Ebert, H. Teichert, P. Strauch, T. Kolb, H. Seifert, J. Wolfrum, Proc. Combust. Inst. **30**, 1611–1618 (2005)

9. H. Teichert, T. Fernholz, V. Ebert, Appl. Opt. **42**, 2043–2051 (2003)

10. M. Schoenung, R.K. Hanson, Combust. Sci. Technol. **24**, 227–237 (1980)

11. R.M. Mihalcea, D.S. Baer, R.K. Hanson, Appl. Opt. **36**, 8745–8752 (1997)

12. J. Wang, M. Maiorov, D.S. Baer, D.Z. Garbuzov, J.C. Connolly, R.K. Hanson, Appl. Opt. **39**, 5579–5589 (2000)

13. M.E. Webber, J. Wang, S.T. Sanders, D.S. Baer, R.K. Hanson, Proc. Combust. Inst. **28**, 407–413 (2000)

14. B.J. Kirby, B.K. Hanson, Proc. Combust. Inst. **28**, 253–259 (2000)

15. M.J. Castaldi, A.M. Vincitore, S.M. Senkan, Combust. Sci. Technol. **107**, 1–19 (1995)

16. T. Melton, Proc. Combust. Inst. **27**, 1631–1637 (1998)

17. A.V. Mokhov, B.A.V. Bennett, H.B. Levinsky, M.D. Smooke, Proc. Combust. Inst. **31**, 997–1004 (2007)

18. A. Mokhov, S. Gersen, H. Levinsky, Chem. Phys. Lett. **403**, 233–237 (2005)

19. F. Xu, Combust. Flame **71**, 593–650 (2000)

20. H. Tsuji, I. Yamaoka, Proc. Combust. Inst. **13**, 723–731 (1971)

21. T.S. Norton, K.C. Smyth, J.H. Miller, M.D. Smooke, Combust. Sci. Technol. **90**, 1–34 (1993)

22. I. Yamaoka, H. Tsuji, Proc. Combust. Inst. **16**, 1145–1154 (1977)

23. H. Tsuji, Prog. Energy Combust. Sci. **8**, 93–119 (1982)

24. V. Sick, in *Symposium (International) on Combustion*, vol. 23 (1990), pp. 495–501

25. S. Wagner, B.T. Fisher, J. Fleming, V. Ebert, Proc. Combust. Inst. **32**, 839–846 (2009)

26. S. Schäfer, M. Mashni, J. Sneider, A. Miklos, P. Hess, H. Pitz, K.-U. Pleban, V. Ebert, Appl. Phys. B **66**, 511–516 (1998)

27. H.E. Schlosser, J. Wolfrum, V. Ebert, B.A. Williams, R.S. Sheinson, J.W. Fleming, Proc. Combust. Inst. **29**, 353–360 (2002)

28. C. Schulz, A. Dreizler, V. Ebert, J. Wolfrum, in *Handbook of experimental fluid mechanics*, ed. by C. Tropea, A. Yarin, J. Foss (Springer, Berlin, 2007), pp. 1241–1316

29. A.R. Awtry, J.W. Fleming, V. Ebert, Opt. Lett. **31**, 900–902 (2006)

30. A.R. Awtry, B.T. Fisher, R.A. Moffatt, V. Ebert, J.W. Fleming, Proc. Combust. Inst. **31**, 799–806 (2007)

31. E. Schlosser, J. Wolfrum, L. Hildebrandt, H. Seifert, B. Oser, V. Ebert, Appl. Phys. B **75**, 237–247 (2002)

32. L.S. Rothman, I.E. Gordon, A. Barbe, D.C. Benner, P.F. Bernath, M. Birk, V. Boudon, L.R. Brown, A. Campargue, J.-P. Champion, J. Quant. Spectrosc. Radiat. Transfer **110**, 533–572 (2009)

33. L.S. Rothman, I.E. Gordon, R.J. Barber, H. Dothe, R.R. Gamache, A. Goldman, V.I. Perevalov, S.A. Tashkun, J. Tennyson, J. Quant. Spectrosc. Radiat. Transfer **111**, 2139–2150 (2010)

34. J. Brubach, M. Hage, J. Janicka, A. Dreizler, Proc. Combust. Inst. **32**, 855–861 (2009)

35. U. Maas, Appl. Math. **3**, 249–266 (1995)

36. U. Maas, J. Warnatz, Combust. Flame **74**, 53–69 (1988)

37. S. Wagner, M. Klein, T. Kathrotia, U. Riedel, T. Kissel, A. Dreizler, V. Ebert, Appl. Phys. B **107–3**, 585–589 (2012)

38. J.A. Nwaboh, O. Werhahn, D. Schiel, Appl. Phys. B **103**, 947–957 (2010)

39. B.J. Kirby, R.K. Hanson, Appl. Phys. B **507**, 505–507 (1999)

40. A. Singh, M. Mann, T. Kissel, J. Brübach, A. Dreizler, Flow Turbul. Combust. (2012). doi:10.1007/s10494-011-9384-6

41. A.V. Mokhov, H.B. Levinsky, C.E. van der Meij, R.A.A.M. Jacobs, Appl. Opt. **34**, 7074–7082 (1995)